

# New Velocity Transformation Based on Compressibility-Corrected Total Stress

Hanju Lee,<sup>1</sup> Pino M. Martín,<sup>1, a)</sup> and Owen J.H. Williams<sup>2</sup>

<sup>1)</sup>*Department of Aerospace Engineering, University of Maryland, College Park, MD 20742, USA*

<sup>2)</sup>*William E. Boeing Department of Aeronautics and Astronautics, University of Washington, Seattle, WA 98195, USA*

(Dated: 24 January 2022)

A new mean velocity transformation for compressible boundary layer flow is derived. We identify the effects of density fluctuations and integrate these effects into the derivation of the transformation. In-depth analysis of compressibility effects from density fluctuations is enabled by direct numerical simulation data existing in the literature and from the CRoCCo laboratory. The compressible and incompressible flow data include wall-cooling, semi-local Reynolds numbers ranging from 800 to 34000 and Mach numbers ranging from subsonic to 12. The role, significance and physical mechanisms connecting density fluctuations to the momentum balance and to the viscous, turbulent and total stresses are presented. Density-fluctuation corrected formulations are derived from these insights. We identify the significant properties that thus-far are neglected in the derivation of velocity transformations: (1) the Mach-invariance of the near-wall momentum balance of the density-fluctuation-corrected total stress, and (2) the Mach-invariance of the relative contributions by the density-fluctuation-corrected viscous and Reynolds stresses to the total stress. The proposed velocity transformation integrates both properties into a single transformation equation and successfully demonstrates a collapsing of all currently considered compressible cases onto to the incompressible law of the wall. Analyses of the log-layer intercept and the slope demonstrate that the transformation parameters are well within the bounds reported for incompressible data. Based on the physics embedded in the two scaling properties, the success of the newly proposed transformation is attributed to considering the effect of the viscous stress, Reynolds stress, mean density and, lastly, density fluctuations, in a single transformation form.

Keywords: Turbulence | Law of the Wall | Compressible Turbulent Boundary Layer | Mean Velocity Scaling | Density Fluctuation | Hypersonic Flow

## I. INTRODUCTION

Hypersonic flow is an area of interest that has received much attention by the fluid mechanics community in recent years as we move towards faster transport methods such as space travel and hypersonic civilian transport vehicles. In particular, a mean velocity transformation (MVT) for compressible turbulent boundary layer flow (CTBL) that restores the incompressible law of the wall has been sought to account for variations in thermodynamic variables and compressibility. The main driver behind such efforts was suggested by Morkovin in 1962 who "concluded that for moderate Mach numbers, the essential dynamics of these shear flows will follow the incompressible pattern."<sup>1</sup> This hypothesis suggests that correctly accounting for the variation of thermodynamic variables will restore the incompressible law of the wall for wall-bounded compressible flow.

Over the past few decades, various forms of MVTs for CTBL have been proposed for

---

<sup>a)</sup>Electronic mail: mpmartin@umd.edu

compressible flow<sup>2-7</sup>. Starting with the pioneering work of Van Driest<sup>2</sup>, to the recently proposed viscous stress based transformation by Trettel et al.<sup>3</sup> (TL), all have shown to work only within the domain of their respective applicabilities. The Van Driest (VD) transformation has shown success only in scaling adiabatic wall bounded compressible flow<sup>8-11</sup> with reported weakness in scaling of iso-thermal cases with high near-wall thermal and viscosity gradients<sup>3,7,12-14</sup>. The most successful MVT that accounts for the near-wall viscosity gradient was independently developed by Trettel et al.<sup>3</sup> and Patel et al.<sup>7</sup>. However, despite their initial success in isothermal CTBL cases<sup>15,16</sup> with low semi-local Reynolds,  $Re^*$ , the scaling remains unsuccessful for cases with increasing  $Re^*$  where multiple studies<sup>14,17</sup> report a large scatter in the log layer intercept and the slope for such cases. Where  $Re^* = Re_\tau \sqrt{\bar{\rho}/\rho_w}/(\bar{\mu}/\mu_w)$ ,  $Re_\tau = \rho_w u_\tau \delta/\mu_w$  is the friction-velocity based Reynolds number,  $\rho$  is density,  $u_\tau = \sqrt{\tau_w/\rho_w}$  is the friction-velocity,  $\delta$  is the boundary layer thickness,  $\tau_w = \mu \frac{\partial u}{\partial z}|_w$  is the wall shear stress,  $\mu$  is the dynamic viscosity,  $u$  is the streamwise velocity, and  $z$  is the wall normal coordinate. The overbar denotes Reynolds time averaging and the subscript "w" denotes a wall quantity.

In recent months, Griffin et al.<sup>17</sup> (GFM) developed a total stress based MVT that employs a combination of the viscous stress transformation of Trettel et al.<sup>3</sup> and the quasi-equilibrium assumption based transformation of Zhang et al.<sup>4</sup>. They employ a total stress-based functional form to combine these two transformations, such that they are applied in their region of applicability. In their transformation, the domain of applicability of the quasi-equilibrium model is also extended to the semi-local wall-normal coordinate,  $z^* = z u_\tau \sqrt{\rho_w/\rho}/(\mu/\rho)$ , which was proposed by Huang et al.<sup>18</sup> and has shown to be effective in collapsing turbulence statistics in CTBL within the near-wall region<sup>3,7,9,12,14,17,19,20</sup>. The preliminary results of the total stress based transformation in the study by Griffin et al.<sup>17</sup> are promising and an improvement over previous transformations. However there are questions about the broad applicability of quasi-equilibrium hypothesis on which the GFM transformation is partially based, as well as any sensitivities to a broader range of flow conditions (Reynolds numbers and heat transfer). The intercept and the slope of MVT proposed by Griffin et al.<sup>17</sup> are examined in the present paper for an even broader set of conditions.

The transformation by Zhang et al.<sup>4</sup> is derived from the turbulent kinetic energy equation, and a derivation of MVT from the momentum equation perspective is also worthy of attention. Wu et al.<sup>6</sup> examined the total stress from the momentum equation perspective to derive their MVT. This study, however, relies on Prandtl's mixing length hypothesis<sup>21</sup> for the prediction of Reynolds stress and requires *a priori* information of the onset locations for the buffer and log layers. Such requirements make the use of their transformation hard to apply in practice. While relying on the Mach-invariance of the total stress in the momentum equation may be more practical, data show a Mach variance in the total stress and the breakdown of the near wall momentum balance for CTBLs, as classically described. Namely, for high  $Re^*$  number and high Mach number, the data show that the Reynolds stress is greater than the wall shear stress, albeit slightly<sup>9,10,14,19</sup>. This result indicates possible compressibility effects that must be considered to assess the Mach-invariance of the total stress and to derive MVT from the momentum equation perspective.

The CRoCCo CTBL database includes a wide range of  $Re^*$  approximately spanning from 800 to 34000 and is used in the present study to scrutinize the effects of compressibility on CTBL flows at high semi-local Reynolds number. In the present study, the compressibility effects are examined in the context of the thin shear layer (TSL) momentum approximation, which we modify from its classical form to represent the data across the compressible parameter space. After the relative importance of compressibility effects is analyzed, we integrate the new findings into a mean velocity transformation that enables the collapse of data across a wide range of CTBL conditions.

## II. SIMULATION DETAILS AND CTBL DATABASE

The governing equations, numerical methods, boundary conditions and initialization procedures used to gather the high-fidelity CRoCCo Lab database for this study are well documented and verified in previous studies<sup>22–25</sup>. The computational database used for this study is summarized in Table I.

All simulations are low-enthalpy, non-reacting conditions. All simulations use calorically perfect air as the working fluid except for the M10T3 which are calorically perfect Nitrogen( $N_2$ ). The boundary layer edge Mach number ranges from 3 to 12 to highlight the Mach number effects and, most notably, the semi-local friction Reynolds number,  $Re^*$ , approximately ranges from 800 to 34000, a broader range than previously compiled datasets. The  $T_w/T_r$  ratio as well as the wall heat transfer rate,  $B_q = q_w/(\rho_w C_p u_\tau T_w)$ , ranges from 0.2 to 1.0 and from 0 to -0.17, respectively, to highlight the wall temperature effects. In this paper,  $q$  is the surface heat flux,  $C_p$  is the heat capacity at constant pressure and  $T$  is the mean temperature. The boundary layer edge Mach number is listed under  $M_e$  and the wall temperature  $T_w$  is given as a fraction of the adiabatic recovery temperature  $T_r = T_e(1 + 0.9M_e^2(\gamma - 1)/2)$  where  $\gamma$  is the heat capacity ratio. The dimensional values of the boundary layer edge density, temperature and velocity as well as the wall density are provided. Several Reynolds numbers are provided including  $Re_\theta \equiv \rho_e U_e \theta / \mu_e$  where  $\theta$  is the momentum thickness and  $\rho_e$ ,  $U_e$ , and  $\mu_e$  are the boundary layer edge density, velocity, and dynamic viscosity respectively;  $Re_{\delta_2} \equiv \rho_e U_e \theta / \mu_w$  as the ratio of the freestream momentum  $\rho_e U_e^2$  to the wall shear stress  $\tau_w$  (approximated as  $\mu_w U_e / \theta$ ); The friction Reynolds number at wall conditions,  $Re_\tau$  varies between 475 and 825. All values of Reynolds number listed in Table I are measured at the outlet plane of the computational domain. The locations of the outlet plane  $x_o/\delta$  are provided in table II where  $\delta$  is the thickness of the boundary layer at 99% of the freestream velocity measured at the outlet plane.

The computational domain size, grid resolution, and simulation duration of the datasets listed in Table I are provided in Table II. The outer dimensions of the computational boxes are given in units of  $\delta$  measured at the outlet plane. All boundary layers are run on a long domain of approximately 20 to 30 times the outlet boundary layer thickness. The domain width varies among the runs but ranges between 5 and  $10\delta$ . All runs use spanwise periodicity. Grid resolutions are listed in units of the inner viscous length scale  $z_\tau = \mu_w / \rho_w u_\tau$  as indicated by the '+' superscript. The computational grids are made with constant spacing in the streamwise and spanwise directions ( $\Delta x^+$  and  $\Delta y^+$ ). Geometric stretching is used in the wall-normal direction where  $z_k^+ = z_2^+(\chi^{k-1} - 1)/(\chi - 1)$  and  $k$  indicates the wall-normal grid index so that the finest resolution is at the wall surface. The first grid point away from the wall is  $z_2^+$  and the factor  $\chi$  determines the rate of stretching. The grid resolution of the DNS runs has been shown to be sufficient for the current DNS computational method and at the given flow conditions in previous publications. In particular see Martin *et al.*<sup>22</sup>, Duan *et al.*<sup>9,19,25,26</sup>, as well as the references listed in Table I for the individual runs. All runs from Table I use the recycle/rescale method of Xu & Martin<sup>23</sup> to assign the inflow boundary conditions; all with the exception of M7T5-L and M12T5-L. For these two cases, a separated auxiliary long-box boundary layer simulation was run and solution at the outlet of that box was interpolated in time and three-dimensional space onto the inlet of the '-L' runs. The two additional auxiliary boundary layer runs are M7T5 and M12T5 and these provide the inflow condition for the M7T5-L and M12T5-L cases respectively. The auxiliary boundary layers are themselves run using the recycle/rescale method. Note that M7T5 and M12T5 necessarily have the same freestream and wall boundary conditions as the corresponding '-L' cases.

For the statistical analysis, time signals of primitive flow variables are collected from the outlet plane of each run. The total sample time in outer time units  $t(U_e/\delta)$  are provided in Table II. No statistics are collected from the auxiliary boundary layer runs and so the sample time information is irrelevant for cases M7T5 and M12T5. The incompressible channel flow DNS database of Lee *et al.*<sup>27</sup> and Bernardini *et al.*<sup>28</sup> with  $Re_\tau$  ranging approximately from

1000 to 5200 is listed in table III to be used as reference IBTL cases.

### III. DENSITY FLUCTUATION IN COMPRESSIBLE BOUNDARY LAYER

#### A. Breakdown of the Classical Momentum Balance

To probe the possible effects of compressibility on thermodynamic properties suggested in various papers<sup>9,10,14,19</sup>, we examine the TSL momentum equation. In this case we assume that the stream-wise derivatives are negligible, the fluctuations of thermodynamic variables are small, pressure gradient across the boundary layer is small and the magnitude of convection terms is negligible near the wall.

$$1 = \tau_{VS}^+ - \tau_{RS}^+ \quad (1)$$

where the superscript "+" denotes the non-dimensionalization by the wall quantity, where  $\tau_{VS}^+ = \bar{\mu} \frac{\partial \bar{u}}{\partial z} / \tau_w$  and  $\tau_{RS}^+ = \overline{\rho u' w'} / \tau_w$  are the non-dimensional viscous and Reynolds stresses, respectively. Reynolds averaging is used instead of Favre averaging to identify and analyze compressibility terms such as density fluctuations. The classical momentum balance denoted by 1 in the left hand side of Eq.1 is expected to hold near the wall for zero pressure gradient boundary layers if Morkovin's hypothesis is valid.

The momentum balance is considered in Fig. 1c where  $\tau_{TS}^+ = \tau_{VS}^+ - \tau_{RS}^+$  denotes the non-dimensionalized total stress. As expected, the total stress for the ITBL cases in table III agree with the classical momentum balance. However, the balance is not observed for many CTBL cases from the current database, due to higher peak turbulent shear stress  $\tau_{RS}^+$  (see Fig. 1b). This result broadens the breakdown of the classical near wall momentum balance also reported in some previous studies<sup>9,10,14,19</sup>. A close examination of Fig.1c shows correlation between the peak value of  $\tau_{RS}^+$  and Reynolds number,  $Re^*$ . While a further study is required to verify this correlation, it is hypothesized that the breakdown of the classical momentum balance is due to compressibility. Two possible compressibility effects not considered by Eq.1 result from density and pressure fluctuations. In our case, the influence of pressure fluctuations in the inner layer are negligible, following Coleman et al.<sup>12</sup>. Furthermore, the domain of application for this assumption has been extended to the hypersonic Mach number regime recently by Duan et al.<sup>29</sup>. Another recent study by Huang et al.<sup>30</sup> suggests that density fluctuations become more significant in high Mach number conditions citing the differences between Reynolds averaged and Favre averaged turbulent shear stress.

Extending the TSL momentum equation to include density fluctuation effects results in equation,

$$1 = \tau_{VS}^+ - \tau_{RS}^+ - \underbrace{\left( \frac{\overline{\bar{w} \rho' u'} + \overline{\rho' u' w'}}{\tau_w} \right)}_{\zeta^+} \quad (2)$$

which reveals two additional non-dimensionalized density fluctuation terms lumped together as  $\zeta^+ = (\overline{\bar{w} \rho' u'} + \overline{\rho' u' w'}) / \tau_w$ . Both of the terms of  $\zeta$  have been found to be non-negligible for the current database, indicating that the wall normal average and fluctuation velocity term are similar in magnitude to each other.

#### B. The Role and the Mechanism of Density Fluctuation

The role of  $\zeta^+$  is evaluated by first considering the Reynolds shear stress,  $\tau_{RS}^+$ . It is well known that the role of  $\tau_{RS}^+$  in the boundary layer is to decelerate the flow. When the

TABLE I. Boundary layer edge and wall parameters of DNS database.

Case	Viscosity Law	$M_e$	$U_e$	$T_e$	$T_w/T_r$	$-Bq$	$Re_\theta$	$Re_{\delta_2}$	$Re_\tau$	$Re^*$	$u_\tau$	$\rho_w$	$\rho_e$	line&symbol
			m/s	K							$m \cdot s^{-1}$	$kg \cdot m^{-3}$	$kg \cdot m^{-3}$	
M3T5	Power	3.0	882.5	220	1.0	0.0	3480	1760	530	1650	44.5	0.0366	0.0917	— ●
M5T5	Power	4.9	1472	225	1.0	0.0	7450	1980	470	3870	81.5	0.0182	0.0968	— ●
M7T5-L	Power	6.9	2069	224	1.0	0.0	15600	2830	550	9450	115.9	0.00969	0.0926	— ●
M12T5-L	Power	11.7	3612	236	1.0	0.0	46800	3880	550	33990	213.1	0.0038	0.1015	— ●
M5T3	Power	4.9	1477	222	0.5	0.05	4650	2054	610	2350	68.0	0.0324	0.0950	— ◆
M5T1	Power	5.0	1498	223	0.2	0.17	1620	1650	830	800	48.4	0.0973	0.0951	— ★
M10T3	Keyes(N2)	9.1	1410	58.6	0.5	0.11	7565	1745	491	4827	63.0	0.0079	0.0403	— ◆

TABLE II. Computational domain size and grid resolution for the DNS data. Datasets with case name ending in ‘-L’ use inflow interpolation from an auxiliary long-box run. All other cases use the rescaling method of Xu & Martin<sup>23</sup> for inflow assignment. Starred datasets (\*) indicate auxiliary simulations. ~ indicates extended sampling location by the auxiliary simulation.

Case	$N_x$	$N_y$	$N_z$	$\delta$	$L_x/\delta$	$L_y/\delta$	$L_z/\delta$	$\Delta x^+$	$\Delta y^+$	$z_2^+$	$\chi$	$tU_e/\delta$	$x_o/\delta$
				mm									
M3T5	1820	880	110	9.3	28.7	5.7	7.5	8.3	3.4	0.32	1.063	143	26.8
M5T5	1820	880	110	16.6	27.2	5.4	8.1	7.1	2.9	0.26	1.061	134	26.1
M7T5*	1780	1160	110	*	21.1	5.6	6.12	6.6	2.7	0.26	1.061		
M7T5-L	1580	1080	116	39.8	21.0	5.6	7.6	7.4	2.9	0.28	1.061	110	19.7~
M12T5*	1640	1300	110	*	20.4	5.4	5.8	6.8	2.4	0.28	1.060		
M12T5-L	1640	1240	116	125.8	20.4	5.4	7.2	6.8	2.4	0.29	1.060	142	19.8~
M5T3	2032	1080	106	9.0	25.4	5.1	8.4	7.6	2.9	0.32	1.069	199	24.0
M5T1	2080	1648	110	2.5	19.5	5.8	7.3	7.7	2.9	0.29	1.069	190	18.5
M10T3	1920	1680	112	17.8	30.3	10.2	10.7	7.8	2.9	0.31	1.065	93	29.0

TABLE III. Incompressible Channel Flow DNS Database

Case	$Re_\tau$	line&symbol	Reference
LM5200	5186	—■	27
LM2000	1994	- - -◆	27
LM1000	1000	⋯⋯★	27
BOP4100	4079	- - -●	28

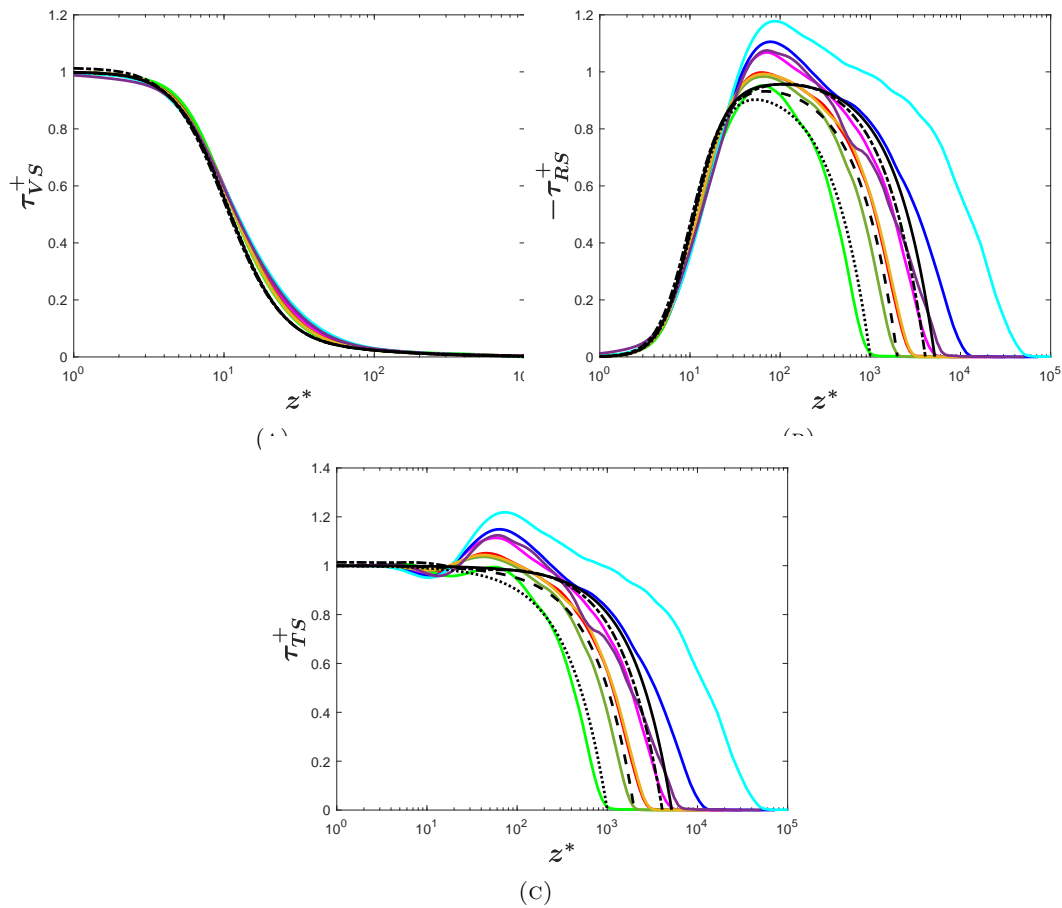


FIG. 1. Non-dimensionalized (A) Viscous stress,  $\tau_{VS}^+$ , (B) Reynolds stress,  $\tau_{RS}^+$ , (C) total stress,  $\tau_{TS}^+$ , are plotted against the semi-local wall normal coordinate,  $z^*$ . Corresponding stresses from ITBL flow references are included for comparison. References for lines colors and styles as well as references for the database are included in table I and III

wall-normal velocity fluctuation,  $w'$ , is positive, lower momentum from the bottom layer is brought to the higher-momentum upper layer. This causes a negative streamwise velocity fluctuation, resulting in a negative  $\overline{u'w'}$ . The opposite occurs for the case of negative  $w'$ , and thus the resulting  $\tau_{RS}^+$  is also negative. The role of the density fluctuation term,  $\zeta^+$ , is the opposite. Plotted in Fig.2, the density fluctuation term is positive in the bulk of the buffer layer and the log layer, hinting that its role is to partially hinder the momentum deceleration induced by  $\tau_{RS}^+$ , and it also indicates that the density fluctuation and the instantaneous  $\overline{u'w'}$  share the same sign. The suggested interpretation is therefore that the fluid inertia opposes the turbulence mixing. That is, instantaneous negative density fluctuations work to reduce the exchange of momentum between the two parcels of fluid at two wall normal

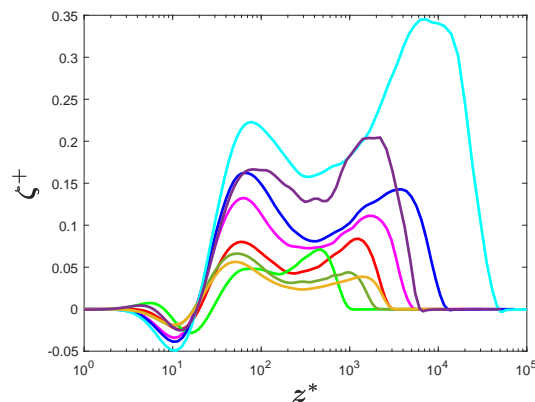


FIG. 2. Sum of the density fluctuation terms,  $\zeta^+$ , versus semi-local wall normal coordinate,  $z^*$ . References for line colors and styles as well as references for the database are included in table I.

locations, opposing the full effect of the deceleration by  $\tau_{RS}^+$ .

### C. Generalized Wall Momentum Balance Equation

We further investigate the extent of the compressibility effects due to density fluctuations. At first glance in Fig. 2, the magnitude of  $\zeta^+$  is significant throughout the inner layer. Noticeably, the magnitude of the first peak which is located at the lower edge of the log layer suggests that  $\zeta$  ranges from 4% to 22% of the wall shear stress and that density fluctuations must be considered for an accurate statement of momentum balance. This influence has not been as noticeable for many previous hypersonic datasets due to the increased contribution of the viscous stress resulting in reductions in the the peak turbulent shear stress for low Reynolds number. In other words, the influences of density fluctuations and low Reynolds number on the Reynolds shear stress are opposite, masking the presence of non-negligible density fluctuations. In the outer layer, an even higher second peak in  $\zeta^+$  indicates a greater influence of density fluctuations in the outer layer. From Fig. 2, we find that CTBL data with increasingly high  $Re^*$  correlate with increased values of  $\zeta^+$  and thus increased density fluctuation effects, as noted previously.

Given that a non-negligible density fluctuations also exist in the viscous layer, albeit smaller than the log layer, a density fluctuation correction to both  $\tau_{VS}^+$  and  $\tau_{RS}^+$  is desirable. Rearranging terms in Eq. 2, a density fluctuation corrected form of Eq. 1, or generalized form of the wall momentum balance equation, can be derived:

$$1 = \frac{\tau_{VS}^+ - \tau_{RS}^+}{\alpha} = \tau_{VS,\alpha}^+ - \tau_{RS,\alpha}^+ \quad (3)$$

where  $\alpha = 1 + \zeta^+$  is a new density fluctuation correction, and  $\tau_{VS,\alpha}^+ = \tau_{VS}^+/\alpha$  and  $\tau_{RS,\alpha}^+ = \tau_{RS}^+/\alpha$  are the density-corrected non-dimensionalized viscous and Reynolds stresses, respectively. For brevity, the terms "density fluctuation correction" and " $\alpha$  correction" will be used interchangeably. By construction, when compressibility effects due to density fluctuations are minimal, Eq. 3 reverts back to Eq. 1. Equation 1 already accounts for variations in mean fluid properties, which has been verified to be sufficient to represent the momentum balance in CTBL with low  $Re^*$ <sup>8,12,14</sup>.

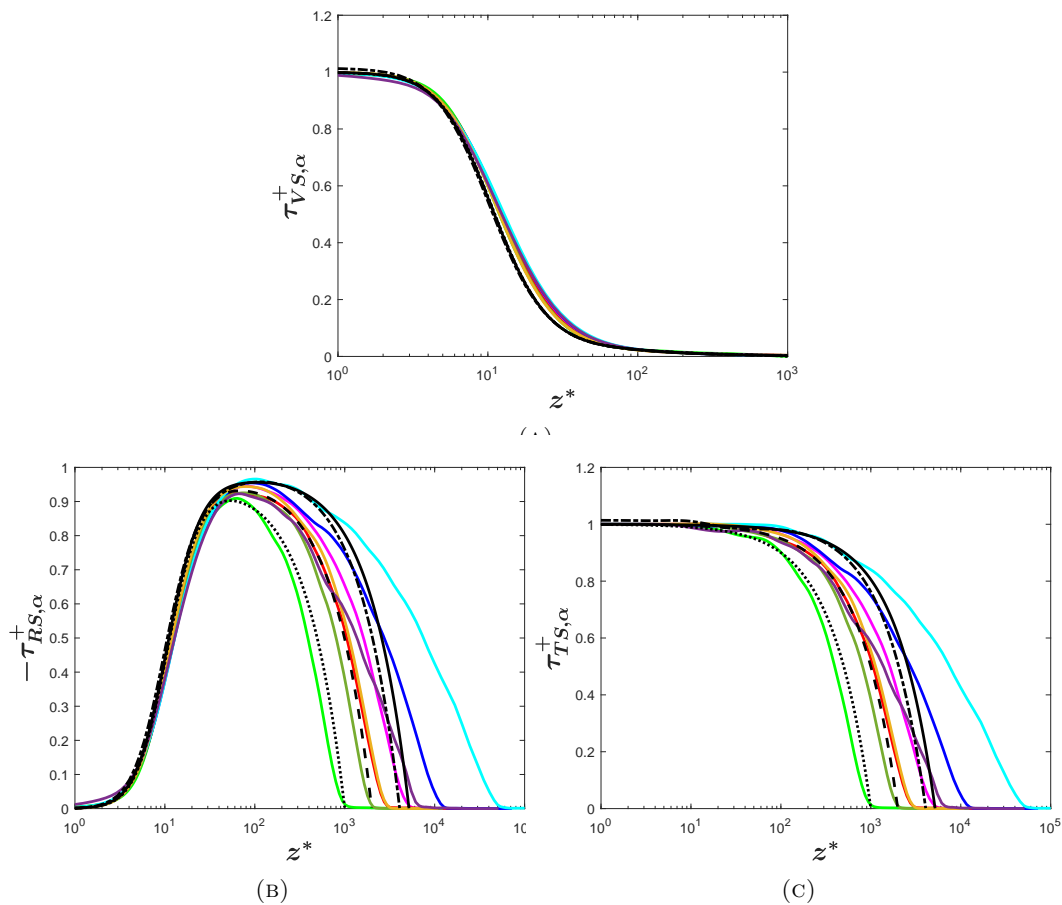


FIG. 3. Non-dimensionalized density fluctuation corrected (A) viscous stress,  $\tau_{VS,\alpha}^+$ , (B) Reynolds stress,  $\tau_{RS,\alpha}^+$ , and (C) total stress,  $\tau_{TS,\alpha}^+$  are plotted against the semi-local wall normal coordinate,  $z^*$ . Corresponding stresses from ITBL flow references are plotted for comparison. References for line colors and styles as well as references for the database are included in table I and III.

#### D. Effect of Density Fluctuations on Stresses

The variation of  $\alpha$ -corrected stresses is shown in Fig.3. For all cases, the  $\alpha$ -corrected total stress remains extremely close to the wall shear stress (i.e. a value of 1 when nondimensionalized) across the inner layer and deviating at higher  $z^*$  for higher  $Re^*$ , as would be expected for ITBLs. Critically, for all CTBL cases considered, we observe a level of Mach-invariance in the total stress  $\tau_{TS,\alpha}$  that is enforced by the near-wall momentum balance. This result suggests the possible use of the  $\alpha$  corrected total stress for the derivation of a generalized MVT.

Comparison of  $\tau_{RS}^+$  and  $\tau_{RS,\alpha}^+$  in Fig. 1b and Fig. 3b reveals significant improvements. Resulting turbulent shear stresses are seen to behave quite similarly to the incompressible profiles of Modesti and Pirozzoli<sup>15</sup>. Best comparisons are seen to occur when compressible  $Re^*$  is matched to incompressible  $Re_\tau$  (i.e. M5T1 is compared to LM1000, M3T5, M3Ad, and M5T3; M5T5 is compared to LM2000, M10T3, and M7T5-L; and M12T5-L is compared to LM5200). For all cases, the peak scaled Reynolds stress now stays below one, consistent with incompressible theory. Similarly, the peak  $\alpha$ -corrected Reynolds shear stress also increases with Reynolds number as it becomes a greater proportion of the total stress as would be expected for ITBLs<sup>27,31</sup>. The overall result of the effects describe indicates an

improvement of the Mach-invariance in  $\tau_{RS,\alpha}^+$ .

At first glance, the comparison of  $\tau_{VS,\alpha}^+$  and  $\tau_{VS,\alpha}^+$  in Fig. 1a and Fig. 3a does not seem to indicate discernible improvement. However, upon closer examination, above the buffer layer  $\tau_{VS,\alpha}^+$  collapses CTBL data better and all CTBL data systemically move modestly closer to the incompressible results. It should also be noted that, as reported in<sup>3,7</sup>, the viscous stress for CTBL and ITBL show a high degree of similarity in the viscous layer and, as seen earlier,  $\zeta$  is less substantial in this region.

Given the discussion above on  $\tau_{VS,\alpha}^+$  and  $\tau_{RS,\alpha}^+$ , it is not surprising that accounting for density fluctuations restores the expected characteristics of the total stress as shown in Fig.3c. The magnitude of  $\tau_{TS,\alpha}^+$  exhibits a satisfying collapse across the ITBL and CTBL data. This result advocates for a new wall coordinate scaling that improves the individual collapse of viscous and Reynolds stress at least for  $z^* \leq 10^2$ .

As a concluding remark on the effect of density fluctuations on the total stress, a few observations important to the derivation of a new MVT must be reiterated. When all thermodynamic properties important to zero pressure gradient CTBL are accounted for, namely the mean property gradients and density fluctuations, the Mach invariance of  $\tau_{TS,\alpha}^+$  is enforced by the near wall momentum balance. Moreover for CTBLs, the degree of Mach-invariance for the viscous and Reynolds stresses is significantly improved with the  $\alpha$  correction, indicating that the relative contributions from the viscous and Reynolds stresses to the total stress remain relatively Mach-invariant in the inner layer. These two important observations indicate that there are two types of Mach invariance embedded within  $\tau_{TS,\alpha}^+$ , namely (1) the Mach-invariance of the near wall momentum balance of the density fluctuation corrected total stress and (2) the Mach-invariance of the relative contributions from the density fluctuation corrected viscous and Reynolds stresses to the total stress.

#### IV. TOTAL STRESS BASED VELOCITY TRANSFORMATION

In recent months, a new total stress based MVT has been proposed by Griffin et al.<sup>17</sup>. Their transformed velocity profile is shown in Fig. 4a and shows a good collapse to the law of the wall. Their success is attributed to the use of a total-stress-based balance to combine the viscous stress based transformations by Trettel et al.<sup>3</sup> and the quasi-equilibrium based transformation of Zhang et al.<sup>4</sup> at locations where the respective assumptions are valid. The exact mathematical form of the total-stress-based transformation,  $S_t^+$ , is given in Eq.4, where  $S_{TL}^+ = \mu^+ \partial u^+ / \partial z^+$  denotes non-dimensionalized mean shear transformed according to Trettel et al.<sup>3</sup> and  $S_{eq}^+ = \frac{1}{\mu^+} \frac{\partial u^+}{\partial z^*}$  denotes the non-dimensionalized mean shear transformed according to Zhang et al.<sup>4</sup>. Equation 4 can also be derived from the total stress representation of the mean shear as shown in Eq. 5.

$$S_t^+ = \frac{\tau_{TS}^+ S_{eq}^+}{\tau_{TS}^+ + S_{eq}^+ - S_{TL}^+} \quad (4)$$

$$\tau_{TS}^+ = S_t^+ \left( \frac{\tau_{VS}^+}{S_{TL}^+} + \frac{\tau_{RS}^+}{S_{eq}^+} \right) \quad (5)$$

In the study of Griffin et al.<sup>17</sup>, they utilize a CTBL database with  $Re^*$  approximately ranging from 200 to 4900 and Mach number ranging from 2 to 14. They present the error relative to the incompressible transformation. The database of the current paper allows us to test the GFM transformation over a wider range of  $Re^*$ , including a range of diabatic conditions (see table I). Comparisons are made with both the incompressible cases of table III and the compressible database of Zhang et al.<sup>14</sup> that was also utilized by Griffin et al.<sup>17</sup>. The LM5200 ITBL was used by Griffin et al.<sup>17</sup> for their incompressible law of the wall baseline.

In contrast to Griffin et al. we choose to examine the influence of the transformation

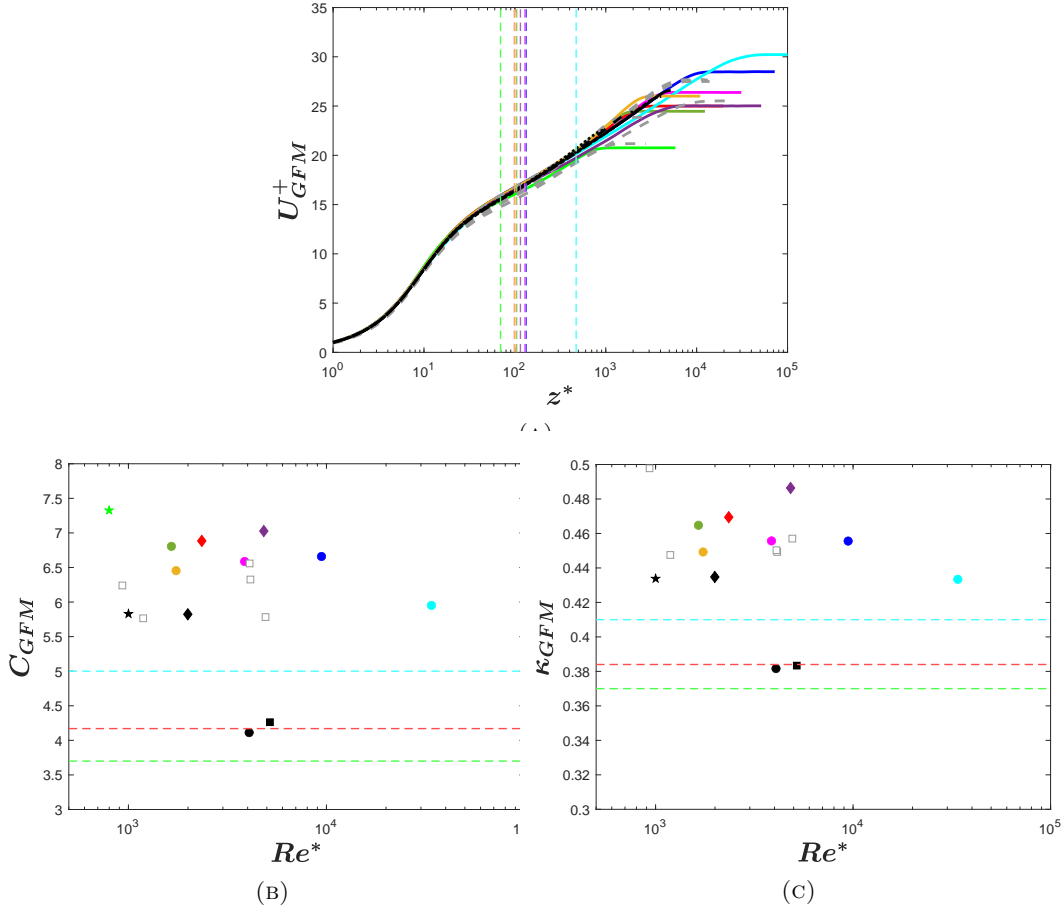


FIG. 4. Griffin et al.<sup>17</sup> (A) Velocity transformation versus semi-local wall normal coordinate,  $z^*$ , (B) Intercept of the Log Layer, (C) Von Kármán Constant,  $\kappa$ , versus Semi local Reynolds Number,  $Re^*$ . Classical incompressible law of the wall velocity profiles, intercepts and  $\kappa$  of the log layer calculated from the incompressible channel flow database are included for comparison. References for colors and styles of lines and symbols as well as references for the CTBL and ITBL database are included in table I and III unless otherwise noted hereafter. Dashed grey lines in (A) and empty grey squares in (B) and (C) are publicly available CTBL database of Zhang et al.<sup>14</sup>. The vertical dashed lines in (A) indicate the wall normal coordinate at which the intercept and  $\kappa$  were calculated (Colors match the corresponding CTBL cases with the reference to the colors in table I). The horizontal dashed lines in (B) and (C) indicate variability in the intercept and  $\kappa$ , respectively, reported in<sup>32</sup>, (dashed cyan line, superpipe), (dashed red line, boundary layer) and (dashed green line, channel).

on the variation in slope and intercept of the log layer. These parameters are determined using the pre-multiplied mean shear as suggested by Lee et al.<sup>27</sup>, given by  $\beta = z^* \frac{dU^+}{dz^*}$ , where  $U^+$  is the transformed mean velocity of interest. If there is a logarithmic layer, the pre-multiplied mean shear will have a plateau, or constant-valued region. To determine the location of the plateau,  $\frac{d\beta}{dz^*}$  is calculated from  $z^*$  of 30 to  $z/\delta < 0.2$ , where  $\delta$  is the wall normal coordinate at the location where mean velocity is 99% of the edge. The  $z^*$  location at the minimum value of  $\frac{d\beta}{dz^*}$  is used as the characteristic location for the log layer.

The log layer intercept and slope for the GFM transformation are shown in Fig. 4b and Fig. 4c, where  $C$  is the intercept and  $\kappa$  is 1/slope or the Kármán constant. The calculated "characteristic locations" of the logarithmic portion of each profile are also shown in Fig.

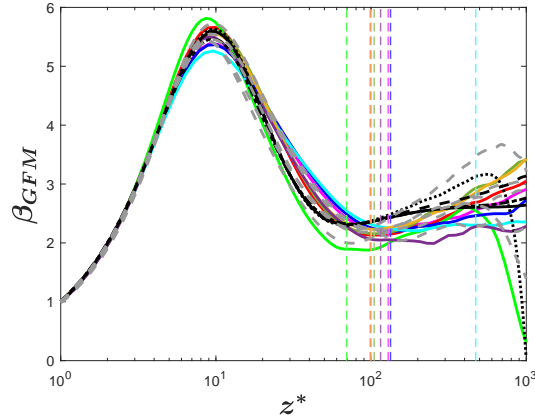


FIG. 5. Pre-multiplied mean shear,  $\beta_{GFM}$ , based on GFM transformation versus semi-local wall normal coordinate. Pre-multiplied mean shear of LM5200 and BOP4100 is calculated from the classical incompressible law of the wall velocity profile and plotted as incompressible reference for comparison. The references for line colors and styles as well as the references for the database are included in table I and III unless otherwise noted hereafter. The vertical dashed lines indicate the wall normal coordinate at which the log layer parameters were calculated (Colors match the corresponding CTBL cases with the reference to the colors in table I). The dashed grey lines are publicly available CTBL database of Zhang et al.<sup>14</sup>.

4a.

The slope and intercept derived from the GFM transformation are not seen to correspond closely to the range of values commonly reported for ITBLs for higher Reynolds numbers. Both  $\kappa$  and intercept are seen to be larger under this transformation. For most cases the slope and intercept are also larger than the low Reynolds number incompressible cases of cases of Lee and Moser<sup>27</sup>. The GFM transformed data at very low  $Re^*$  show the greatest deviations from the incompressible cases as would be perhaps be expected. A further examination of the pre-multiplied mean shear, which is plotted in Fig. 5, that the collapse for the GFM mean velocity profile in Fig. 4a is observed only because Mach-invariance of the pre-multiplied mean shear is somewhat satisfactory up to the onset of the plateau region. However, the Mach-invariance of  $\beta$  quickly deteriorates in the plateau region, where it is expected to show the most logarithmic behavior, resulting in incorrect intercepts and slopes for the log layer. While higher  $Re^*$  cases show larger regions of logarithmic behavior, it is unclear if the correspondence of slope and intercept with incompressible data will improve significantly for the CTBLs at some combination of high  $Re^*$  or  $Re_\tau$ .

We examine the reasons for the above variability of slope and intercept by exploring validity of the three assumptions undertaken in the derivation of the transformation by Zhang et al.<sup>4</sup>, namely: the Mach-invariance of the Favre averaged enstrophy and of the Reynolds stress; the difference between the Favre and Reynolds averaged representations of the Reynolds stress; and the ratio of the Favre averaged turbulent kinetic energy (TKE) production and viscous dissipation terms. Here double prime denotes the turbulent fluctuations with respect to Favre average, and tilde denotes the Favre averaging. For brevity, Einstein notation is used to express the terms pertaining to the TKE equation in this section, where the definition of  $v$  is the velocity in the direction determined by the indices,  $i$  and  $k$ .

While not shown here, it is confirmed that the Mach-invariance of the Favre averaged enstrophy suggested in<sup>10</sup> holds for the CTBL cases listed in table I. However, recall that the Reynolds averaged shear stress in Fig. 1b is not Mach-invariant in the log layer. It is also not shown but confirmed that the Favre averaged Reynolds stresses of CTBL cases listed in table I show no qualitative differences to the Reynolds averaged shear stresses in

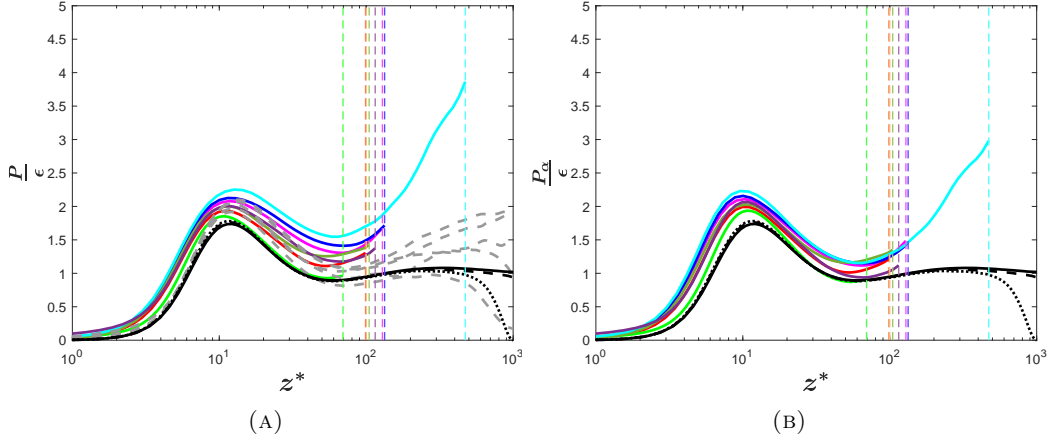


FIG. 6. (A) The ratio of the TKE production ( $P$ ) and viscous dissipation ( $\epsilon$ ), and (B) the ratio of the  $\alpha$  corrected TKE production ( $P_\alpha$ ) and the viscous dissipation ( $\epsilon$ ) versus semi-local wall normal coordinate,  $z^*$ . The vertical dashed lines indicate the wall normal coordinate at which the log layer parameters were calculated (Colors match the corresponding CTBL cases with the reference to the colors in table I). Dashed grey lines in (A) are the ratio obtained from the publicly available CTBL database of Zhang et al.<sup>14</sup>. The references for line colors and styles as well as the references for the database are included in table I unless otherwise noted.

Fig. 1b. Finally, Fig. 6a plots the ratio of the Favre averaged TKE production ( $P$ ) and the Reynolds averaged viscous dissipation ( $\epsilon$ ), mathematically given by  $\overline{\rho v_i'' v_k''} \partial \tilde{v}_i / \partial x_k$  and  $\overline{\tau_{ik}'} \partial v_i' / \partial x_k$ , respectively. For the CTBL cases, the Mach-invariance of the ratio quickly deteriorates throughout the buffer and log layers. Therefore, the GFM representations of the log layer intercept and slope are thought to deteriorate because two of the three underlying assumptions used to derive the ZH transformation, are invalid. Thus, the GFM use of the quasi-equilibrium assumption becomes inaccurate in the log layer.

The Favre averaged TKE production term can also be density fluctuation corrected, as shown in Eq. 6. The ratio of the  $\alpha$ -corrected Favre averaged TKE production ( $P_\alpha$ ) and the Reynolds averaged viscous dissipation ( $\epsilon$ ) is plotted in Fig. 6b. The density corrected ratio exhibits better Mach-invariance characteristics than the uncorrected ratio in Fig. 6a. While not pursued in this study, combined with the improved scaling characteristics of  $\alpha$ -corrected Reynolds stress in Fig. 3b, it is suggested that the ZH transformation and, therefore, the GFM transformation can be improved by considering the density fluctuation terms.

$$P_\alpha = \overline{\rho v_i'' v_k''} \frac{\partial \tilde{v}_i}{\partial x_k} + \overline{\rho' v_i'' v_k''} \frac{\partial \tilde{v}_i}{\partial x_k} \quad (6)$$

## V. PROPOSED NEW TOTAL STRESS-BASED TRANSFORMATION

In an effort to develop a generalized MVT for CTBL, two scaling properties of  $\tau_{TS,\alpha}^+$  have been identified: (1) Mach-invariance of the  $\tau_{TS,\alpha}^+$  magnitude dictated by the near wall momentum balance and (2) Mach-invariance of the relative contributions of the constituting viscous and turbulent stresses in  $\tau_{TS,\alpha}^+$ . In the new transformation, we incorporate both of these characteristics. Let  $R_{vs}$  and  $R_{rs}$  be the ratio of viscous and Reynolds stress to the

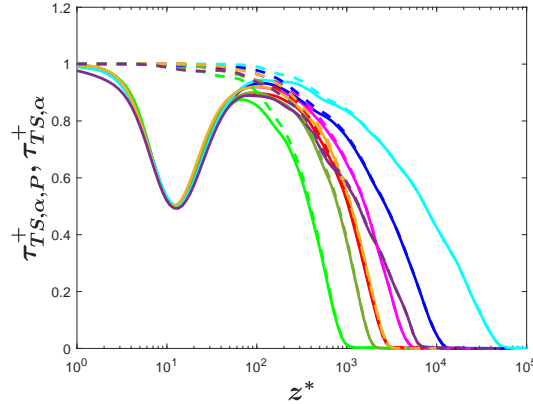


FIG. 7. Solid line indicates proportionally accurate  $\alpha$  corrected total stress,  $\tau_{TS,\alpha,P}^+$ , and dashed line indicates  $\alpha$  corrected total stress,  $\tau_{TS,\alpha}^+$  plotted for comparison. References for lines colors as well as references for the database are included in table I.

total stress respectively:

$$\begin{aligned} R_{vs} &= \tau_{VS,\alpha}^+ / \tau_{TS,\alpha}^+ \\ R_{rs} &= -\tau_{RS,\alpha}^+ / \tau_{TS,\alpha}^+ \end{aligned} \quad (7)$$

The Mach-invariance in the relative contributions of  $\tau_{VS,\alpha}^+$  and  $\tau_{RS,\alpha}^+$  to  $\tau_{TS,\alpha}^+$  is first ensured by multiplying  $R_{vs}$  and  $R_{rs}$  by the viscous and Reynolds stress terms to arrive at an equation of similar form to Eq. 3:

$$\tau_{TS,\alpha,P}^+ = R_{vs}\tau_{VS,\alpha}^+ + R_{rs}(-\tau_{RS,\alpha}^+) \quad (8)$$

Where  $\tau_{TS,\alpha,P}^+$  denotes proportionally accurate  $\alpha$ -corrected total stress. In this approach, Eq. 8 provides an accurate proportional representation of each stress to the total stress at any wall-normal coordinate location. This mathematical treatment decouples the viscous friction  $\tau_{VS,\alpha}^+$  and turbulent mixing  $\tau_{RS,\alpha}^+$  effects. Figure 7 plots  $\tau_{TS,\alpha,P}^+$ . The proportionally accurate  $\alpha$  corrected total stress,  $\tau_{TS,\alpha,P}^+$ , shows the accurate proportionality by construction, i.e. it enforces the proportionality of the relative contributions by the constituting stresses. Also plotted here is the  $\alpha$  corrected total stress,  $\tau_{TS,\alpha}^+$ , which enforces the first scaling property, i.e. the scaling of the magnitude given by the near wall momentum balance. Because both  $\tau_{VS,\alpha}^+$  and  $\tau_{RS,\alpha}^+$  exhibit a high degree of Mach-invariance for CTBL cases, as shown in Fig. 3a and Fig. 3b,  $\tau_{TS,\alpha,P}^+$  exhibits exceptional scaling in the inner layers as well. Moreover, as suggested previously in Fig. 3c,  $\tau_{TS,\alpha}^+$  exhibits the high degree of Mach-invariance. However,  $\tau_{TS,\alpha,P}^+$  fails to account for the Mach-invariance dictated by the near wall momentum balance in  $\tau_{TS,\alpha}^+$ , as demonstrated by  $\tau_{TS,\alpha,P}^+$  failing to remain unity in the buffer region.

To restore the near-wall momentum balance,  $\tau_{TS,\alpha,P}^+$  can be mathematically transformed in a manner similar to that of Griffin et al.<sup>17</sup>. They represent the total stress in Eq. 5 in terms of mean shear quantities,  $S_t^+$ ,  $S_{TL}^+$  and  $S_{eq}^+$ . By construction,  $S_t^+$  is the mean shear that exhibits the characteristics of either  $S_{TL}^+$  in the near-wall limit, or of  $S_{eq}^+$  in the log layer. Equation 5 preserves the magnitude of the total stress prescribed by the viscous and the Reynolds stresses. Note  $S_{TL}^+$  is identical to  $\tau_{VS,\alpha}^+$ , and it is quite accurate in its description of the viscous layer. However, based on the observations of the previous sections, we propose the replacement of  $S_{eq}^+$  in Eq. 5 with the mean shear form of  $\tau_{TS,\alpha,P}^+$ . In this way, the new total-stress-based mean shear will preserve the magnitude of the total stress while exhibiting the scaling characteristics of  $\tau_{TS,\alpha,P}^+$ .

To transform  $\tau_{TS,\alpha,P}^+$  into the mean shear form, the resulting Reynolds stress term is square rooted and divided by  $\kappa z^*$  on a dimensional basis

$$S_{TS,\alpha,P}^+ = R_{vs}\tau_{VS,\alpha}^+ + \frac{\sqrt{R_{rs}(-\tau_{RS,\alpha}^+)}}{\kappa z^*}, \quad (9)$$

where  $S_{TS,\alpha,P}^+$  denotes the proportionally accurate mean shear based on the total stresses. We have used  $\tau_{VS,\alpha}^+$  in place of  $S_{TL}^+$  to include the effect of the density fluctuations on the viscous stress. Notice, the non-dimensionalized viscous stress is identical to its mean shear form<sup>3,7</sup>, and thus the use of  $\tau_{VS,\alpha}^+$  in place of  $S_{TL}^+$  is appropriate. We now replace  $S_{eq}^+$  with  $S_{TS,\alpha,P}^+$  to include the Mach-invariance of the proportionality of  $\tau_{TS,\alpha,P}^+$ . The density fluctuation corrected forms of the viscous and Reynolds stresses are prescribed to account for the density fluctuation in the stresses. The resulting equation is Eq. 10

$$\tau_{TS,\alpha}^+ = S_{TS,\alpha,P,M}^+ \left( \frac{\tau_{VS,\alpha}^+}{\tau_{VS,\alpha}^+} - \frac{\tau_{RS,\alpha}^+}{S_{TS,\alpha,P}^+} \right) \quad (10)$$

where  $S_{TS,\alpha,P,M}^+$  denotes the mean shear that preserves both the proportionality of the constituting stresses in  $\tau_{TS,\alpha}^+$  and the magnitude of  $\tau_{TS,\alpha}^+$ . Equation 10 can be rearranged to solve for the mean shear,  $S_{TS,\alpha,P,M}^+$ :

$$S_{TS,\alpha,P,M}^+ = \frac{\tau_{TS,\alpha}^+}{1 - \tau_{RS,\alpha}^+/S_{TS,\alpha,P}^+} \quad (11)$$

$S_{TS,\alpha,P,M}^+$  can be integrated with respect to the semilocal wall unit,  $z^*$ , from the wall to the freestream to obtain the transformed velocity,  $U_\alpha^+ = \int S_{TS,\alpha,P,M}^+ dz^*$ . Thus, the mean shear,  $S_{TS,\alpha,P,M}^+$  in Eq.11 is the newly proposed transformation that preserves the two scaling properties of  $\tau_{TS,\alpha}^+$  as described in the beginning of the section. Moreover, by the definition of each constituting term and by construction, this transformation includes the effects of mean density variation, density fluctuations, and viscous and Reynolds stresses. All four effects have been verified to be important in CTBL flows.

It is noted that the mathematical treatment of Reynolds shear stress in Eq. 9 transforms  $\tau_{TS,\alpha,P}^+$  into the mean shear form. While this mathematical treatment is the same as that of the mixing length hypothesis, in that the Reynolds stress is also square-rooted and divided by the mixing length,  $\kappa z^*$ , the present paper does not endorse the mixing length hypothesis. The current mathematical construct is strictly derived on dimensional grounds.

The proposed mathematical treatment is consistent with Townsend's attached eddy hypothesis<sup>33-35</sup>, which depicts energy containing eddies as organized motions of fluids attached to the wall. Thus, the induced velocity fluctuations by these eddies are proportional to  $z^*$ :

$$\begin{aligned} u' &= z^* f(z^*) \\ w' &= z^* g(z^*) \end{aligned} \quad (12)$$

Where  $f(z^*)$  and  $g(z^*)$  are currently non-linear functions with dimension of  $1/s$ . We can deduce from Eq. 12 that the Reynolds stress is proportional to the square of wall distance as:

$$u'w' = (z^*)^2 h(z^*) \quad (13)$$

Where  $h(y^*)$  is a non-linear function with a dimension of  $1/s^2$ . Equation 9 invokes the same dimensional bases. In addition, notice that the von Kármán constant,  $\kappa$ , is a relic to mimic the 'slope' of the incompressible log law. Both the mathematical treatment for the Reynolds stress and the new transformation will result in a collapsing velocity profile, no matter what value of  $\kappa$  is used. For the velocity transformation and for all cases in this paper, we use the value of 0.381 for  $\kappa$  from LM5200 in table III, as reported in<sup>27</sup>.

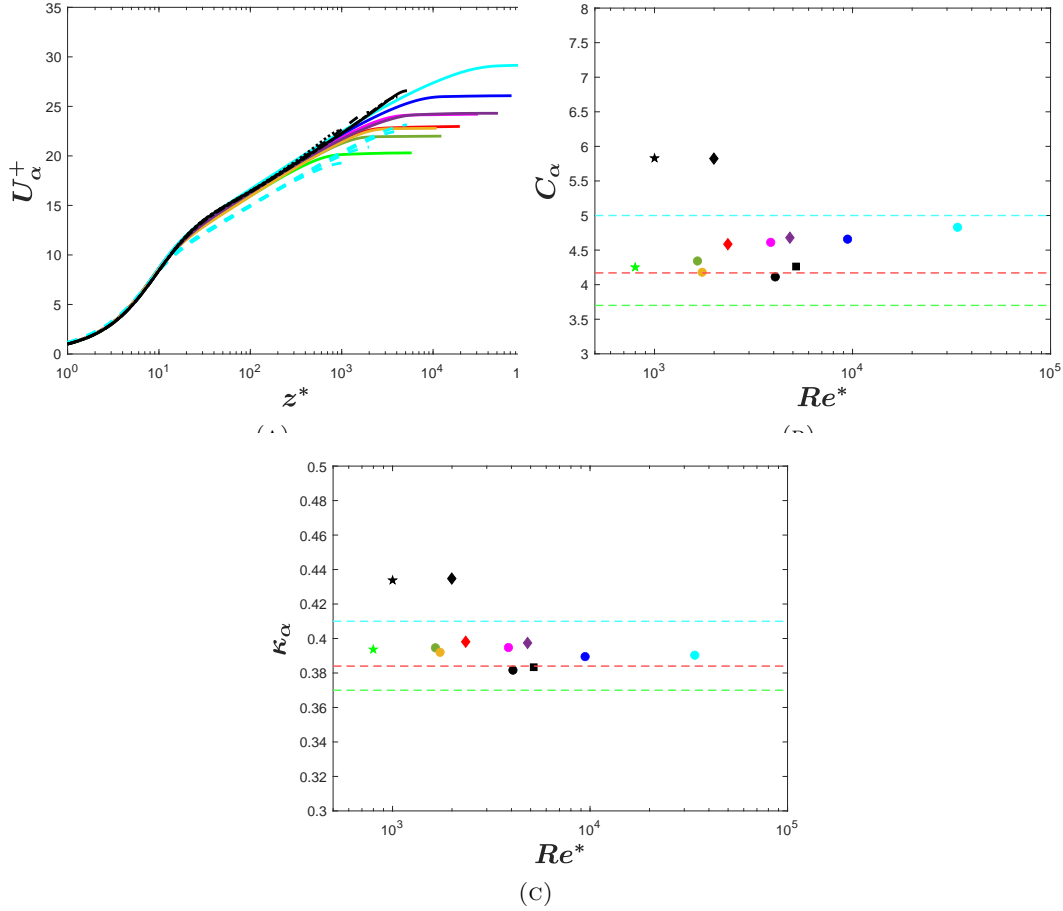


FIG. 8. (A) The presently-proposed velocity transformation versus semi-local wall normal coordinate,  $z^*$ . (B) Intercept and (C) von Kármán constant,  $\kappa$ , of the log layer plotted against semi-local Reynolds number. The ITBL flow data listed in table III are transformed using a conventional law of the wall and are plotted for comparison in (A),(B) and (C). References for line colors and styles and symbols as well as references for the database are included in table I and III unless noted otherwise hereafter. Dashed cyan lines in (A) denote the velocity profiles of the ITBL flow data transformed by the proposed MVT. Horizontal lines in (B) and (C) denote variability in the intercept and  $\kappa$ , respectively, reported in<sup>32</sup>, (dashed cyan line, superpipe), (dashed red line, boundary layer) and (dashed green line, channel).

## VI. DISCUSSION OF RESULTS

The transformed mean velocity profiles for CTBL and ITBL data according to Eq. 11 are shown in Fig. 8a. ITBL data is transformed using the proposed transformation by assuming  $\alpha$  to be 1 and setting the mean thermodynamic properties to the wall value. Also included here is the classical law of the wall derived from the overlap argument. The proposed transformation collapses all of the CBTL velocity profiles to the classical incompressible result; supersonic and hypersonic, adiabatic and non-adiabatic. In addition to the qualitative examination of the mean velocity profile, both the log law intercept and slope for all CTBL and ITBL data are calculated by using the pre-multiplied mean shear to locate the characteristic location of the log layer as was done for the GFM transformation. Note that slope and the intercept of the ITBL data in Fig. 8b and Fig. 8c are calculated from the classical law of the wall profiles. With an exception of low  $Re_\tau$  incompressible cases, Fig. 8b and

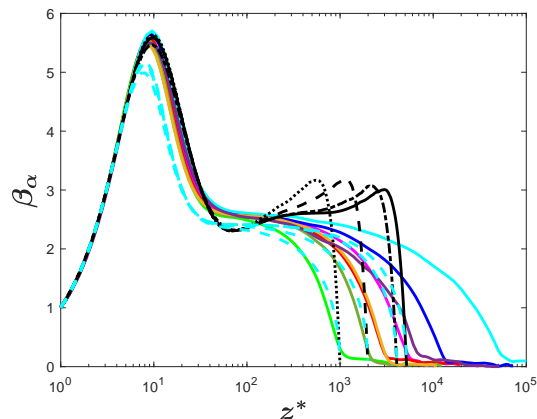


FIG. 9. Pre-multiplied mean shear,  $\beta_\alpha$ , based on the present mean velocity transformation versus semi-local wall normal coordinate,  $z^*$ . The pre-multiplied mean shear is calculated for ITBL cases (see table III) using the conventional law of the wall for comparison. References for line colors and styles as well as references for the database are included in table I and III unless noted otherwise hereafter. Dashed cyan lines indicate the pre-multiplied mean shear of the ITBL cases transformed by the proposed MVT.

Fig. 8c show a very small variability when compared to highest Reynolds number ITBL (LM5200 and BOP4200).

To quantitatively compare the scatter in the log law intercept and slope for the proposed and GFM transformations, we use coefficients of variation (CoV), which is defined as the standard deviation divided by the mean of the data of interest. Higher CoV values indicate larger scatter. The intercept value for LM5200 and BOP 4100 are also considered. Incompressible cases with lower Reynolds numbers, namely LM1000 and LM2000, are excluded as they deviate from all other cases, likely due to their low Reynolds number and insufficient separation of scales. The CTBL data by Zhang et al.<sup>14</sup> is not included in this comparison as density fluctuation data is needed to perform the transformation and it is not available in the published database. The CoV values of the log law intercepts by the proposed transformation in Fig. 8b and by GFM transformation in Fig. 4b are calculated to be 0.0517 and 0.1401, respectively, representing an approximately three-fold reduction in scatter. The CoV values of  $\kappa$  by the proposed and GFM transformations are calculated to be 0.0115 and 0.0849, respectively. Not only the scatter of  $\kappa$  is improved approximately by eight-fold, the value of the intercepts generated by the proposed transformation overlap the incompressible range considerably better.

The pre-multiplied mean shear is computed for the new MVT,  $\beta_\alpha = z^* \frac{du^+}{dz^*}$ , and plotted in Fig. 9. Note that all CTBL cases exhibit a plateau region starting around  $z^*$  of 30, and extending to higher  $z^*$  for higher  $Re^*$ , indicating an onset of logarithmic behavior right above the buffer layer. For the ITBL cases, the proposed transformation results in mean velocity profiles that collapse all ITBL cases with a long logarithmic layer starting around  $z^*$  of 30 as shown in Fig. 8a. This logarithmic layer can also be confirmed by the existence of the plateau region in  $\beta_\alpha$  for all ITBL cases, as shown in Fig. 9. However, apparent differences in the log layer intercept values can be observed between the CTBL and ITBL cases when the proposed transformation is used, see Fig. 8a. This difference is attributed to the observed deviation of the CBTL  $\tau_{VS,\alpha}$  data from the ITBL data in viscous sublayer, as shown in Fig. 3a. Provided that a successful scaling of the CTBL and ITBL viscous stress is possible in the viscous sublayer, the proposed MVT would be expected to produce a scaled mean velocity profile for both CTBL and ITBL with the same intercept. It is not entirely certain why there are differences between the viscous stresses for the CTBL and ITBL data, and further studies are required to reveal the underlying reason for this deviation.

There exists a known Reynolds number dependence in the classical law of the wall as

demonstrated by different values of the intercept and the slope for low  $Re_\tau$  cases in Fig.8b and Fig.8c. However, as noted earlier, this Reynolds number dependency is not visible for the proposed transformation. Because the proposed transformation is accounting for the relative contributions of viscous and turbulent stresses directly, the new transformation accounts for one of the main sources of low-Reynolds number dependence on the classical law of the wall.

Based on the important compressibility effects including the density fluctuation, previous transformations, i.e. van Driest II<sup>2</sup>, Trettle-Larsson<sup>3</sup>, and Griffin-Zhang-Moin<sup>17</sup>, in one way or another, lack the key physics that are required for a more-complete description of the near-wall flow behavior. The reasons of their success and failure are identified and discussed here with respect to the MVT requirements discussed in this study.

As reported by a number of previous authors<sup>3,7,12,13</sup>, the Van Driest II transformation fails to collapse compressible cold wall data because it lacks a consideration of the viscous stress. Moreover, comparison of  $\tau_{TS}^+$  and  $\tau_{TS,\alpha}^+$  in Fig. 1c and Fig. 3c, respectively, demonstrates that the total stress is truly equal to  $\tau_w$  in the inner layer only when density fluctuations are considered. From this observation, we can conclude that the success of the Van Driest II transformation for adiabatic cases with high  $Re^*$ , which exhibit  $-\tau_{TS}^+$  over 1 as shown in Fig. 1c, is largely attributed to the inaccurate but quite fortunate description of the Reynolds stress where the mean density corrected mixing length hypothesis incorrectly enforces the Reynolds stress to equal  $\tau_w$  in the log layer without considering the density fluctuation effects.

Again, from the new finding that both viscous and Reynolds stresses must be taken into account for the successful development of a velocity transformation, the Trettle-Larsson transformation<sup>3</sup> results in incorrect slope and intercept because it only uses a viscous stress-based mean shear. However, the Reynolds stress dominates in the log layer. As a result, TL lacks the information to appropriately describe turbulence mixing in this region. While not shown here, and in agreement with the finding in<sup>14</sup>, it is confirmed that the TL transformation will be successful only for cases with extremely low  $Re^*$  (i.e. cases with very high viscous effects) and that the intercept and slope of the logarithmic portion of the TL profile increases  $Re^*$ . This confirms the expectation of Griffin et al.<sup>17</sup> that the Trettle-Larsson transformation decreases in accuracy for cases with moderate-to-high  $Re^*$ .

While the transformation of Griffin et al.<sup>17</sup> has shown promising and improved collapse of the mean velocity profiles, the use of quasi-equilibrium model<sup>4</sup> to describe the turbulence in the log layer is not strictly accurate, as demonstrated by the variability and increased log layer intercept and slope results shown in Fig. 4b and Fig. 4c. Moreover, examination of the underlying assumptions in the quasi-equilibrium model suggests that the deficiencies of the GFM transformation are twofold and due to the breakdown of the Mach-invariance in the Reynolds stress, and the Mach-invariance in the ratio of the turbulent kinetic energy production and viscous dissipation terms in the log layer when they are not density-corrected, as shown in Fig. 1b and Fig. 6a, respectively.

Finally, the success of the proposed MVT can be attributed to considering the influence of density fluctuations and the mean property gradients in both the viscous and Reynolds stresses. Two scaling properties, namely, the proportionality and the magnitude-invariance of the  $\alpha$ -corrected total stress, are identified and integrated into the newly proposed MVT. Because this transformation is based on the scaling characteristics of density fluctuation-corrected total stress in the thin shear layer momentum equation, it is expected that the proposed transformation will scale any wall bounded flow that does not violate the momentum balance of the density fluctuation-corrected thin shear layer equation in the viscous, buffer and log layers. Therefore, while caution should be used before applying this transformation in fully developed channel and pipe flows, it is our expectation that this transformation will work equally well in collapsing the velocity profiles for such flows.

## VII. CONCLUSION

In this paper, a density fluctuation-corrected total stress-based velocity transformation has been derived by identifying important characteristics of wall-bounded compressible flows. It is demonstrated that the influence density fluctuations is important and must be considered when to scaling the turbulent stresses in compressible turbulent boundary layer flows. Moreover, through an examination of the effect of the density fluctuations on the viscous and Reynolds stresses, two scaling properties of the density fluctuation-corrected total stress have been identified: Namely, (1) the Mach-invariance of the near-wall momentum balance of the density fluctuation corrected total stress and (2) the Mach-invariance of the proportion of the density fluctuation-corrected viscous and Reynolds stresses to the total stress. A new mean velocity transformation that considers the effects of mean density gradient, both viscous and Reynolds stresses, and the effect of density fluctuations has been derived by accounting for these two scaling properties.

The newly proposed velocity transformation is seen to provide an accurate representation of the logarithmic layer. For a wide range of Mach numbers, Reynolds numbers and heat transfer, the scatter in the intercept and slope of the new transformation are within the bounds found for incompressible flow data. The new transformation is successful because, for the first time, it accounts for the density fluctuation effects in both the viscous and Reynolds stresses. It has been verified that the proposed velocity transformation is successful in collapsing velocity profiles of for all compressible cases described in this study. The collapse of the density fluctuation-corrected viscous and Reynolds stresses provides a semi-empirical form that can be used to apply this transformation as a wall model for CTBL.

## ACKNOWLEDGMENTS

This work was supported in part by the Air Force Office of Scientific Research under award number FA9550-20-1-0085 monitored by Dr. Sarah Popkin, by the National Numerical Evaluation Site for Hypersonics. Computational resources were provided by the Department of Defense under the High Performance Computing Modernization Program (DoD HPCMP) and by the CRoCCo Laboratory at the University of Maryland.

<sup>1</sup>A. Smits and J. Dussauge, *Turbulent shear layers in supersonic flow: Second edition* (Springer New York, United States, 2006).

<sup>2</sup>E. R. V. Driest, "Turbulent boundary layer in compressible fluid," *J. Aeronaut. Sci.* **18**, 145—216 (1951).

<sup>3</sup>A. Trettel and J. Larsson, "Mean velocity scaling for compressible wall turbulence with heat transfer," *Physics of Fluids* **28**, 026102 (2016), <https://doi.org/10.1063/1.4942022>.

<sup>4</sup>Y.-S. Zhang, W.-T. Bi, F. Hussain, X.-L. Li, and Z.-S. She, "Mach-number-invariant mean-velocity profile of compressible turbulent boundary layers," *Phys. Rev. Lett.* **109**, 054502 (2012).

<sup>5</sup>C. Brun, M. P. Boiarciuc, M. Haberkorn, and P. Comte, "Large eddy simulation of compressible channel flow - Arguments in favour of universality of compressible turbulent wall bounded flows," *Theoretical and Computational Fluid Dynamics* **22**, 189–212 (2008).

<sup>6</sup>B. Wu, W. Bi, F. Hussain, and Z.-S. She, "On the invariant mean velocity profile for compressible turbulent boundary layers," *Journal of Turbulence* **18**, 186–202 (2017), <https://doi.org/10.1080/14685248.2016.1269911>.

<sup>7</sup>A. Patel, B. J. Boersma, and R. Pecnik, "The influence of near-wall density and viscosity gradients on turbulence in channel flows," *Journal of Fluid Mechanics* **809**, 793–820 (2016).

<sup>8</sup>S. E. Guartini, R. D. Moser, K. Shariff, and A. Wray, "Direct numerical simulation of a supersonic turbulent boundary layer at mach 2.5," *Journal of Fluid Mechanics* **414**, 1–33 (2000).

<sup>9</sup>L. Duan, I. Beekman, and M. P. Martin, "Direct numerical simulation of hypersonic turbulent boundary layers. part 3. effect of mach number," *Journal of Fluid Mechanics* **672**, 245–267 (2011).

<sup>10</sup>M. Lagha, J. Kim, J. D. Eldredge, and X. Zhong, "A numerical study of compressible turbulent boundary layers," *Physics of Fluids* **23**, 015106 (2011), <https://doi.org/10.1063/1.3541841>.

<sup>11</sup>S. Pirozzoli, F. Grasso, and T. B. Gatski, "Direct numerical simulation and analysis of a spatially evolving supersonic turbulent boundary layer at m=2.25," *Physics of Fluids* **16**, 530–545 (2004), <https://doi.org/10.1063/1.1637604>.

<sup>12</sup>G. N. Coleman, J. Kim, and R. D. Moser, "A numerical study of turbulent supersonic isothermal-wall channel flow," *Journal of Fluid Mechanics* **305**, 159–183 (1995).

- <sup>13</sup>H. Foysi, S. Sarkar, and R. Friedrich, “Compressibility effects and turbulence scalings in supersonic channel flow,” *Journal of Fluid Mechanics* **509**, 207–216 (2004).
- <sup>14</sup>C. Zhang, L. Duan, and M. M. Choudhari, “Direct numerical simulation database for supersonic and hypersonic turbulent boundary layers,” *AIAA Journal* **56**, 4297–4311 (2018).
- <sup>15</sup>D. Modesti and S. Pirozzoli, “Reynolds and Mach number effects in compressible turbulent channel flow,” *International Journal OF Heat and Fluid Flow* **59**, 33–49 (2016).
- <sup>16</sup>J. Yao and F. Hussain, “Turbulence statistics and coherent structures in compressible channel flow,” *Phys. Rev. Fluids* **5**, 084603 (2020).
- <sup>17</sup>K. P. Griffin, L. Fu, and P. Moin, “Velocity transformation for compressible wall-bounded turbulent flows with and without heat transfer,” *Proceedings of the National Academy of Sciences* **118** (2021), 10.1073/pnas.2111144118, <https://www.pnas.org/content/118/34/e2111144118.full.pdf>.
- <sup>18</sup>P. Huang, G. Coleman, and P. Bradshaw, “Compressible turbulent channel flows: Dns results and modelling,” *Journal of Fluid Mechanics* **305** (1995), 10.1017/S0022112095004599.
- <sup>19</sup>L. Duan and M. Martín, “Direct numerical simulation of hypersonic turbulent boundary layers. part 4. effect of high enthalpy,” *Journal of Fluid Mechanics* **684**, 25 – 59 (2011).
- <sup>20</sup>A. Patel, J. W. R. Peeters, B. J. Boersma, and R. Pecnik, “Semi-local scaling and turbulence modulation in variable property turbulent channel flows,” *Physics of Fluids* **27**, 095101 (2015), <https://aip.scitation.org/doi/pdf/10.1063/1.4929813>.
- <sup>21</sup>L. Prandtl, “Bericht über untersuchungen zur ausgebildeten turbulenz,” *Z. Angew. Math. Mech.* **5**, 136–139 (1925).
- <sup>22</sup>M. Martín, “Direct numerical simulation of hypersonic turbulent boundary layers. part 1. initialization and comparison with experiments,” *Journal of Fluid Mechanics* **570**, 347 – 364 (2007).
- <sup>23</sup>S. Xu and M. P. Martín, “Assessment of inflow boundary conditions for compressible turbulent boundary layers,” *Physics of Fluids* **16**, 2623–2639 (2004), <https://doi.org/10.1063/1.1758218>.
- <sup>24</sup>M. P. Martín, E. M. Taylor, M. Wu, and V. G. Weirs, “A bandwidth-optimized WENO scheme for the effective direct numerical simulation of compressible turbulence,” *Journal of Computational Physics* **220**, 270–289 (2006).
- <sup>25</sup>E. M. Taylor, M. Wu, and M. P. Martín, “Optimization of nonlinear error for weighted essentially non-oscillatory methods in direct numerical simulations of compressible turbulence,” *J. Comput. Phys.* **223**, 384–397 (2007).
- <sup>26</sup>L. Duan, I. Beekman, and M. P. Martín, “Direct numerical simulation of hypersonic turbulent boundary layers. part 2. effect of wall temperature,” *Journal of Fluid Mechanics* **655**, 419–445 (2010).
- <sup>27</sup>M. Lee and R. D. Moser, “Direct numerical simulation of turbulent channel flow up to  $Re_\tau \approx 5200$ ,” *Journal of Fluid Mechanics* **774**, 395–415 (2015).
- <sup>28</sup>P. O. M. Bernardini, S. Pirozzoli, “Velocity statistics in turbulent channel flow up to  $retau=4000$ ,” *Journal of Fluid Mechanics* **742**, 171–191 (March 2014).
- <sup>29</sup>L. Duan, M. M. Choudhari, and C. Zhang, “Pressure fluctuations induced by a hypersonic turbulent boundary layer,” *Journal of Fluid Mechanics* **804**, 578–607 (2016).
- <sup>30</sup>J. Huang, G. L. Nicholson, L. Duan, M. M. Choudhari, and R. D. Bowersox, “Simulation and modeling of cold-wall hypersonic turbulent boundary layers on flat plate,” in *AIAA Scitech 2020 Forum* (2020) <https://arc.aiaa.org/doi/pdf/10.2514/6.2020-0571>.
- <sup>31</sup>J. A. Sillero, J. Jiménez, and R. D. Moser, “One-point statistics for turbulent wall-bounded flows at reynolds numbers up to  $\delta^+ \approx 2000$ ,” *Physics of Fluids* **25**, 105102 (2013), <https://doi.org/10.1063/1.4823831>.
- <sup>32</sup>H. M. Nagib and K. A. Chauhan, “Variations of von kármán coefficient in canonical flows,” *Physics of Fluids* **20**, 101518 (2008), <https://doi.org/10.1063/1.3006423>.
- <sup>33</sup>A. Townsend, “The Structure of the Turbulent Boundary Layer,” *Proceedings of the Cambridge Philosophical Society* **47**, 375–395 (1951).
- <sup>34</sup>A. Townsend, “Equilibrium Layers and Wall Turbulence,” *Journal of Fluid Mechanics* **11**, 97–120 (1961).
- <sup>35</sup>A.A.Townsend, *The structure of turbulent shear flow* (Cambridge Univ. Press, Cambridge, UK., 1976).